Slip flow Lattice-Boltzmann simulations in ducts and porous media: a full rehabilitation of spurious velocities

M. Aminpour,* A. Scheuermann, and L. Li
Research Group on Complex Processes in Geo-Systems. School of Civil Engineering, The University of Queensland, Brisbane QLD 4072, Australia

S. A. Galindo-Torres
School of Engineering, University of Liverpool, UK

Slip flow in ducts and porous media is simulated using lattice-Boltzmann method incorporated with interfacial force models. The dependence of the results on the viscosity, LBM scheme (D3Q15 and D3Q19) and the relaxation time model (single or multi-relaxation time) is investigated. The severity of spurious velocities (arisen from classic and advanced interfacial force models) is discussed that leads to entirely non-physical results for whole flow rates ($0.027 < Re < 10.7$). A simple method based on superposition of solutions is proposed to fully rehabilitate the simulations. We validate the method by showing the simulations versus analytical solution of slip flow through circular ducts. The validity of the rehabilitated results for porous media applications are also tested through two approaches: First, we show that the rehabilitation method is independent to the force scheme used, *i.e.*, the rehabilitated results are identical in both pore and macro-scales for different force schemes with different distributions of spurious velocities. Second, using an analogy based on the Kozeny-Carman model, we show that the permeability variation in porous media resulted from the flow slippage obtained from rehabilitated simulations is reliable. We argue that to obtain correct results, it is necessary to use the rehabilitation method whenever interfaical force models are used in LB simulations. The results reveal that the permeability of porous media may increase or decrease with positive or negative slippage (repulsive and attractive interfaces), respectively. The permeability enhancement rate increases as the system becomes simpler in its interfaces, *i.e.*, for the same positive slippage of flow, $(\frac{\kappa}{\kappa_{NS}})_{parallel\ plates} > (\frac{\kappa}{\kappa_{NS}})_{square\ ducts} > (\frac{\kappa}{\kappa_{NS}})_{porous\ media}$ (where κ is the permeability and $_{NS}$ denotes no-slip).

I. INTRODUCTION

Fluid flow in porous media is ubiquitous in nature and technology. Applications span many sectors and processes such as oil recovery [1], shale gas production [2], CO_2 storage [3, 4], filtration membranes [5, 6], water treatment [7], fuel cells [8], and microfluidics [9–11]. In most analytical and numerical investigations of natural or artificial porous media, the well-known no-slip boundary condition is applied on the solid surfaces [12]. In recent years, this assumption is shown to fail in many circumstances, including in the presence of interfacial interactions, *e.g.* hydrophobic [13–15] or hydrophilic [16–20] interfaces, and micro/nanofluidics characterized by high Knudsen numbers [21–24]. The importance of the issue is better understood when considering the ubiquity of interfacial interactions. All inorganic minerals of soil, except for dehydroxylated silica are hydrophilic due to the charges and polar groups on their surfaces [25]. However, water repellency is also common for soil and peat which is caused by the organic matter of soil (humic acid) [26]. There is also experimental evidence indicating the existence of a strong interfacial energy imposed to the fluid at the vicinity of many materials, in a long-range fashion [27]. This leads to the formation of a deep surface zone of molecule orientation (a review in [28]). Particularly, the solute-free zone near the hydrophilic surfaces is shown as a long-range zone [29, 30], not only for aqueous solutions but also for other polar liquids [31]. Recently, it has been shown that the pore-scale features could induce significant variations in microscopic flow behavior leading to highly variable transport mechanisms while the macroscopic permeability could remain unchanged [32–34]. Finally, the impact of wettability on the dynamics of drying and drainage [35, 36], the permeability of porous media [37, 38] and oil recovery [39] is well recognized.

On the other hand, the influence of interfacial interactions is more significant when the characteristic size of the medium decreases. There is a large number of applications in nature, technology, biology and medicine where the fluidic systems are downsized [9]. As the ratio of surface-to-volume increases, the physics of microfluidics becomes largely dependent on the surface properties [40]. Therefore, surface interactions characterized by wettability or hydrophobic/hydrophilic behaviour is one of the most important issues determining the resistance of such systems to flow [41, 42].

The apparent slip of flow is the main feature induced by interfacial interactions (a review for the slip of Newtonian liquids is provided in [43]). The slip flow involves the interplay of several physiochemical parameters including the wettability of the solid, shear rate, pressure, electrical properties (*e.g.* ionic strength and polarity), surface roughness, as well as impurities and dissolved gas

* m.aminpour@uq.edu.au

[12]. While it is very difficult to determine all involving parameters precisely, it has been shown that their interplay can be successfully simulated using the lattice-Boltzmann method incorporating the application of local forces at the interfaces [44]. The method has been shown to be appropriate for simulation of slip flow over planar surfaces [45–48].

Although successfully implementable for slip flow investigations, the interfacial force models have certain limitations. A problem known as *spurious currents* or *spurious/parasitic velocities*, emerging in all computational fluid dynamic approaches, has been shown to be linked to the simulation of forces on non-planar (curved) interfaces [49–55]. The spurious velocities are non-physical rotational fluid velocities spreading throughout the domain, especially at the vicinity of the interfaces. Thus a simulation of flow in realistic porous media incorporating interfacial forces is always to some extent affected by spurious velocities. The problem is highlighted when knowing that one of the main reasons for the popularity of the LBM is providing the facility to simulate realistic (complex) pore geometries. In many cases, the spurious velocities may cause entirely non-physical simulation results, particularly when the low-rate (laminar) flow and/or strong interfacial forces are dominant. Researchers have introduced many different computationally demanding ways to mitigate the spurious velocities, *e.g.* higher-order approximation of the gradient term [49, 51, 52, 56–58]. Despite these attempts, the spurious currents are usually reduced only by folds or an order of magnitude and a full remediation is yet to be achieved [44]. For instance, the application of multi-relaxation time model in Ref [59], although decreasing the magnitudes of spurious velocities, has yet led to large non-physical velocities (making any flow simulation non-physical for $Re < 2.3$, with respect to characteristic lengths of the model). Furthermore, in current work, we show that the application of advanced interfacial force models is also insufficient for obtaining the physical results in slip flow simulations.

We propose a simple method to fully rehabilitate the spurious velocities for single-phase fluid flow problems involving interfacial interactions. The method is shown to be accurate enough to determine the pore flow changes in porous media induced by interfacial force. Our simple post-processing rehabilitation method provides a significant accessibility for the lattice-Boltzmann method to a broad area of research, namely, flow simulations in wettable /non-wettable porous media using available interfacial force models.

We validate our method with two different approaches: firstly, we implement two different force models that largely changes the values and distributions of the spurious velocities. Then we show that the rehabilitation method is not affected by the variations of the non-physical velocities, leading to accurately identical rehabilitated velocity fields. Secondly, we propose an analogy between the porous medium and other systems (ducts and plates) in which the spurious velocities are minimal. Then the overall behavior of flow in those systems in presence of attractive/repulsive forces is compared. The rehabilitated results showing the variation of the permeability of porous media is evaluated based on the similarity to other systems, also in comparison with analytical solutions. The results demonstrate that the attractive/repulsive interactions corresponding to negative/positive slip lengths induce reduction/increase of permeability in porous media. The rate of the permeability variation in different systems is also compared.

II. METHODS

A. Lattice-Boltzmann Method

The fluid flow was simulated using the lattice Boltzmann method that solves the discrete Boltzmann equation for a distribution of particles, $f_i(\vec{\boldsymbol{x}}, t)$, on a discrete lattice [60]. For each particle (cell), a set of discrete velocities ($\vec{\boldsymbol{e}}_i$) along discrete paths (i) is assigned and f_i is the probability function of each velocity. Employing D3Q15 scheme, the movement of particles with 15 velocity components are determined, indexed from 0 to 14, the first of which is associated with the rest case with null velocity [61]. The flow density ρ and velocity $\vec{\boldsymbol{u}}$ at a cell position $\vec{\boldsymbol{x}}$ are:

$$\rho(\vec{\boldsymbol{x}}) = \sum_{i=0}^{14} f_i(\vec{\boldsymbol{x}}) \tag{1}$$

$$\vec{u}(\vec{\boldsymbol{x}}) = \frac{\sum_{i=0}^{14} f_i(\vec{\boldsymbol{x}})\vec{\boldsymbol{e}}_i}{\rho(\vec{\boldsymbol{x}})} \tag{2}$$

We also compare the D3Q19 and D3Q19 schemes.

The Boltzmann equation could be solved using an evolution rule [62]:

$$f_i(\vec{\boldsymbol{x}} + \vec{\boldsymbol{e}}_i\delta t, t + \delta t) = f_i(\vec{\boldsymbol{x}}, t) + \Omega_{coll} \tag{3}$$

where t is the current time, δt is the time step and Ω_{coll} is the collision operator. Unless mentioned otherwise, the collision operator utilized here is the widely used Bhatnagar-Gross-Krook (BGK) model with the following form:

$$\Omega_{coll} = \frac{f_i^{eq} - f_i}{\tau} \tag{4}$$

with f_i^{eq} being an equilibrium distribution function and τ being the characteristic relation time. The Navier-Stokes equations are shown to be recovered with having [63]:

$$f_i^{eq} = \omega_i\rho\left(1 + \frac{3\vec{\boldsymbol{e}}_i.\vec{\boldsymbol{u}}}{C^2} + \frac{9(\vec{\boldsymbol{e}}_i.\vec{\boldsymbol{u}})^2}{2C^4} - \frac{3u^2}{2C^2}\right) \tag{5}$$

where $C = \delta_x/\delta_t$ is a characteristic lattice velocity with δ_x being the time step and δ_x, the grid spacing. The weight factor ω_i is also assigned for each direction, the sum of which for all would be unity (see [64]: Table 1

for weight factors of different schemes). The dynamic viscosity of the fluid also determines the relaxation time, τ as

$$\nu = (\tau - 0.5)\frac{\delta_x^2}{3\delta_t} \tag{6}$$

Unless mentioned otherwise, we have kept the magnitude of τ equal to 1 to prevent numerical instabilities [62], where δ_t and δ_x are also kept as unity. A detailed parametric study on the influence of viscosity (and the choice of τ) will be explained in Section III. In this section we also use the multi-relaxation time scheme which is described in Ref. [65].

B. Interparticle pseudopotential models

The methods defining the multi-phase/multi-component interactions in LBM could be categorized into the following three models: the pseudopotential model of Shan and Chen [66, 67], the color gradient model of Gunstensen [68] and the free energy model of Swift et al. [69, 70]. This study adopted the pseudopotential model which is known as the most widely used model in this class, and introduced for interactions of multi-phase [66, 67] and multi-component flow [71] (a review is available in [44]). We incorporated this model to account for the solid boundary interactions with fluid in repulsive or attractive fashion. An improved pseudopotential model known as explicit forcing scheme (EFS) is also developed that is featured with reduction of spurious velociites among other advantages [72]. We also use this method to model the interfacial dynamics as discussed later in Section VIII A.

1. Original Shan Chen pseudopotential model

The way the multicomponent and multiphase forces are implemented in the SC model [66, 67] is similar to the body forces, *e.g.* gravity [73], where a net force is introduced for each cell. The velocity used for the equilibrium function is modified with the net force, $\vec{\boldsymbol{F}}$ as the following:

$$\vec{\boldsymbol{u}} = \vec{\boldsymbol{u'}} + \frac{\tau \vec{\boldsymbol{F}}}{\rho} \tag{7}$$

where $\vec{\boldsymbol{u'}}$ is an effective velocity and $\vec{\boldsymbol{F}}$ is the total force (including interfacial interactions). The fluid-solid repulsion is modeled as

$$\vec{\boldsymbol{F}} = -g_s \rho(\vec{\boldsymbol{x}}) \sum_{i=1} \omega_i s(\vec{\boldsymbol{x}} + \sigma_t \vec{\boldsymbol{e}}_i)\vec{\boldsymbol{e}}_i \tag{8}$$

where g_s is the force factor controlling the intensity of the solid-fluid repulsion and the function s is unity when the neighboring cell is solid and zero otherwise. The attractive force is also modeled with a negative force factor.

2. Explicit forcing scheme

In EFS, rather than through an equilibrium velocity shift as in the original SC model, the force term is directly incorporated into the discrete Boltzmann equation which yields to the following implicit expression [72]:

$$\begin{aligned} f_i(\vec{\boldsymbol{x}} + \vec{\boldsymbol{e}}_i\delta_t, t + \delta_t) - f_i(\vec{\boldsymbol{x}}, t) = \Omega_{coll} \\ + \frac{\delta_t}{2}\left[f_i^F(\vec{\boldsymbol{x}} + \vec{\boldsymbol{e}}_i\delta_t, t + \delta_t) + f_i^F(\vec{\boldsymbol{x}}, t)\right] \end{aligned} \tag{9}$$

where f_i^F is the forcing term added to the function to account for variations due to external forces, and Ω_{coll} is the same as Eq. 4. The forcing term is also defined as [74]:

$$f_i^F = \frac{\vec{\boldsymbol{F}}.(\vec{\boldsymbol{e}}_i - \vec{\boldsymbol{u}})}{\rho C^2} f_i^{eq} \tag{10}$$

with F being the external force. The equilibrium distribution function f_i^{eq} is in the same form as Eq. 5. The momentum substituted in Eq. 5 in SC model is different due to the velocity treatment as per Eq. 7. In the SC model, the external forces are introduced to the distribution function through $\vec{\boldsymbol{u'}}$. Therefor $\vec{\boldsymbol{u'}}$ is an effective momentum. In EFS model, the forces are directly incorporated into the distribution function, thus the $\vec{\boldsymbol{u'}}$ is simply an effective velocity.

With the following transformation applied to Eqs. 4 and 9,

$$\bar{f}_i = f_i - \frac{\delta t}{2} f_i^F \tag{11}$$

we obtain the explicit force scheme expressed as

$$\begin{aligned} \bar{f}_i(x + \vec{\boldsymbol{e}}_i\delta t, t + \delta t) - \bar{f}_i(x, t) \\ = \frac{1}{\tau}\left[f_i^{eq}(x, t) - \bar{f}_i(x, t) - \frac{\delta t}{2} f_i^F\right] + \delta t f_i^F. \end{aligned} \tag{12}$$

III. PARAMETRIC STUDY OF NUMERICAL SIMULATIONS

A. Viscosity-dependence of simulations

We conducted a detailed study on the influence of viscosity (and therefore the relaxation time) on the results. In addition to the Bhatnagar-Gross-Krook (BGK) single-relaxation time model, we also use the multi-relaxation time (MRT) scheme [65]. We also check the influence of different LBM schemes (D3Q15 and D3Q19) when used with the SRT model. With a system of circular duct with different diameters, we also investigate the influence of the characteristic lengths when curved surfaces of the ducts are modeled as zigzag boundaries. The results of simulations when reaching the steady state are shown as mean velocity of flow which is compared to the analytical mean flow (Fig. 1). The viscosities used for the simulations are between 1/30 to 2, equivalent to $0.6 < \tau < 6.5$. From the results, we conclude that:

- For all methods used here (SRT-D3Q15, SRT-D3Q19, MRT-D3Q15), the highest accuracy is obtained for $1 < \tau < 2$.
- For all methods used, the simulation flow rate is less than the analytical value for $\tau < 1$. The simulation flow velocity is larger than the $\langle u \rangle_{Ana}$ for $\tau > 2$ for SRT models, but remains smaller for MRT.
- The viscosity (relaxation time)-dependence of the simulation velocity is generally less for 19-velocity scheme compared to 15-velocity one, and for MRT compared to SRT. MRT has almost the same stability (and accuracy) for the whole viscosity range examined, while the SRT-D3Q15 is less stable than the SRT-D3Q19 for large viscosities.
- For all of the schemes checked here, with a higher resolution of simulations (i.e a larger number of cells per the characteristic length of the system), the error of the velocity decreases leading to less viscosity-dependency and higher accuracy of the results.

B. Simulation iterations

It is worth mentioning that the iteration times required to reach the steady-state conditions are different for different viscosities assigned. If the results are taken from the same time steps, the viscosity-dependence would be exaggerated. As a rule of thumb, the smaller the viscosity, the larger the time iterations needed. The time steps used in our simulations for this part are between 2500 to 35000 for largest and smallest viscosities, respectively. A larger number of iterations are also needed as the number of lattices increases. For a model of $100 \times 25 \times 25$ lattices used for the case of $R = 20$, 2500 time steps were enough to reach the steady-state condition for all viscosities. The largest number of time steps were required for the models with largest sizes and smallest viscosities.

C. No-slip assumption

The no-slip velocity boundary conditions at the fluid-solid interface are usually approximated using the standard bounce-back (SBB) boundary conditions. This model is defined to mimic the momentum reflection of particles when colliding with a solid surface. However, for the standard BB boundary condition, the position of wall is not always obtained at the one-half grid spacing beyond the last fluid node [75]. In the BGK model, the actual position of the wall could be viscosity dependent when the standard BB is applied, as derived from the analytic solutions for the Poiseuille flow [76]. The accuracy of no-slip boundary condition is of the first order of the resolution, and might be low in under-relaxed situations, i.e., when $\tau > 1$ or for the low-resolution simulations. However, it is also shown that the accuracy of the no-slip assumption for bounce-back scheme with halfway wall is of second order that is a high accuracy with acceptable results for Poiseuille flow [76].

The accuracy of the no-slip model in our simulations is indicated in In Fig. 2 through the fitting equations on the no-slip velocity profiles. The erroneous slip velocities when the no-slip model is assumed are in order of 10^{-3} and 10^{-4} compared to the maximum velocity of the flow for the plate spacing of $d = 10$ and $d = 30$, respectively. Compared to the slip velocities obtained from slip flow models, the errors are negligible. The accuracy also improves as the resolution of simulation increases. Given that the resolution of our porous media simulations is comparatively high (at least 68 cells per diameter), we conclude that the models are suitable for no-slip assumptions.

Furthermore, as we are interested in slip flow characterization, the position of the wall is the relative coordinates of the origin for relative variation of the velocity profiles. In our simulations, we consider the fluid cell velocity for the coordinates of the middle of the cell. The wall location is then where the velocity equals to zero for the velocity profile of models with $g_s = 0.0$. This consideration usually places the wall at the edge of the first fluid cell neighboring to solid cells. When $g_s \neq 0$, the variation of the velocity profile is compared to the corresponding wall location for the no-slip assumption.

Finally, in Figs. 4 and 6(d), we show a validation of slip lengths from LBM simulations against analytical solutions. In those figures, it is illustrated that the slip lengths tend to zero for interfacial forces tending to zero. The close agreement of slip velocities in LBM simulations with analytical slip velocities demonstrate the suitability of the models used for both no-slip and slip flow simulations.

IV. SLIPPAGE OF POISEUILLE FLOW

A. Flow between parallel plates

Using the interfacial force schemes, we obtained positive and negative slippage of flow corresponding to repulsive and attractive forces, respectively (Fig. 3). The negative slip is usually associated with the surface roughness which narrows the effective channel width, in addition to the Knudson number or electroosmotic flow [21, 77, 78]. The positive slippage causes an enhanced flow rate with an increase in the effective plate separation [78, 79].

The analytical solution for mean velocity of Poiseuille flow between parallel plates with no-slip surfaces is [80]

$$\langle u \rangle = \frac{d^2}{12\mu} G \tag{13}$$

where G denotes a pressure gradient or body force generating the flow. Application of slip boundary conditions

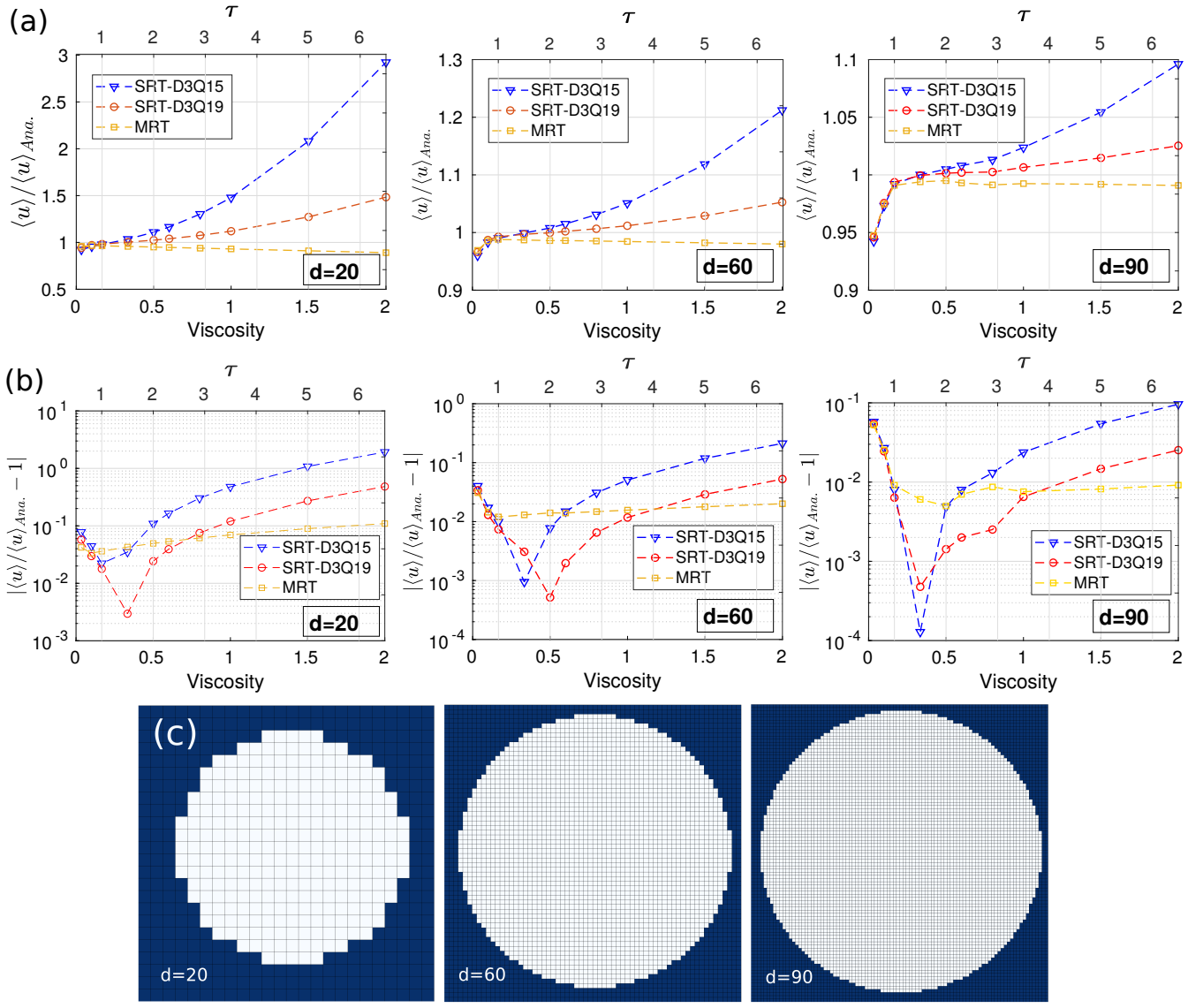

FIG. 1. Viscosity-dependence of the simulations. The normalized mean velocity of the flow through circular ducts (a) and its relative error (b) vs. the viscosity ν in l.u and the relaxation time τ. The lattice resolution is $100 \times (d+5)^2$. The analytical flow mean velocity is given as $\langle u \rangle_{Ana} = R^2 G/(8\mu)$. The cross-section of the models is shown in (c)

at solid surfaces yields the mean flow velocity as [81]

$$\langle u \rangle = \frac{d^2}{12\mu}\left(1 + \frac{6\lambda}{d}\right) G \tag{14}$$

with λ being the slip length (as defined in Fig. 3(a)) and d being the plate separation. Using the interfacial forces controlled with the force factor g_s, LBM simulations induce the slippage of flow with specific slip lengths. The flow rates corresponding to the slip lengths that appear in our LBM simulations exhibit a close agreement with the available analytical solutions (Fig. 4).

B. Flow through polygonal ducts

Analytical solutions for slip flow in polygonal ducts are obtained from separation of variables leading to solutions in the form of infinite series of eigenfunctions [82–84].

For a rectangular duct, as solved by [83], the mean velocity of flow is [84]:

$$\langle u \rangle = \frac{L^2}{\mu} \times \sum_{n=1}^{\infty} \frac{a_n \sin \alpha_n}{\alpha_n^3}\left[1 - \frac{\sinh(\alpha_n b)}{\alpha_n b\big[\cosh(\alpha_n b) + \lambda \alpha_n \sinh(\alpha_n b)\big]}\right] G \tag{15}$$

where one side of the rectangle is $2L$ and the other is

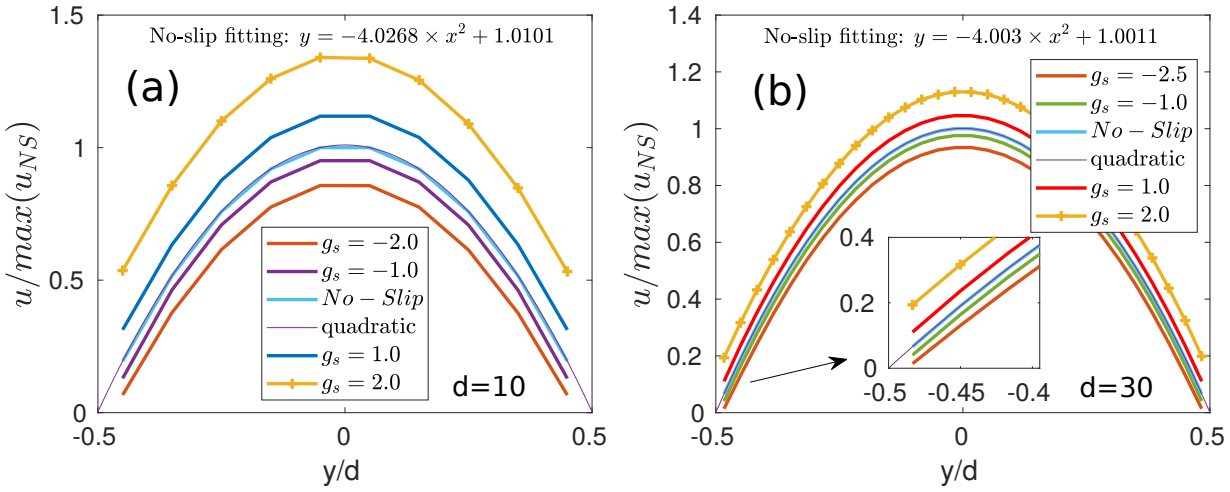

FIG. 2. Evaluation of the no-slip assumption. Velocity profiles of flow between parallel walls with spacing of $d = 10$ (a) and 30 (b) in l.u. Simulations are conducted using SRT-D3Q15 scheme with standard bounce-back boundary conditions at walls. The resolution of simulations is $(d+2) \times 110^2$ lattices.. The no-slip velocity profile is obtained from simulations with no interfacial forces ($g_s = 0$) and bounce-back boundary conditions. The fitting equations on the no-slip velocity profiles indicate the accuracy of the model for the no-slip assumption, leading to erroneous slip velocities of $(3.4 \times 10^{-3}) \times u_{max}$ and $(3.5 \times 10^{-4}) \times u_{max}$ for $d = 10$ and 30, respectively.

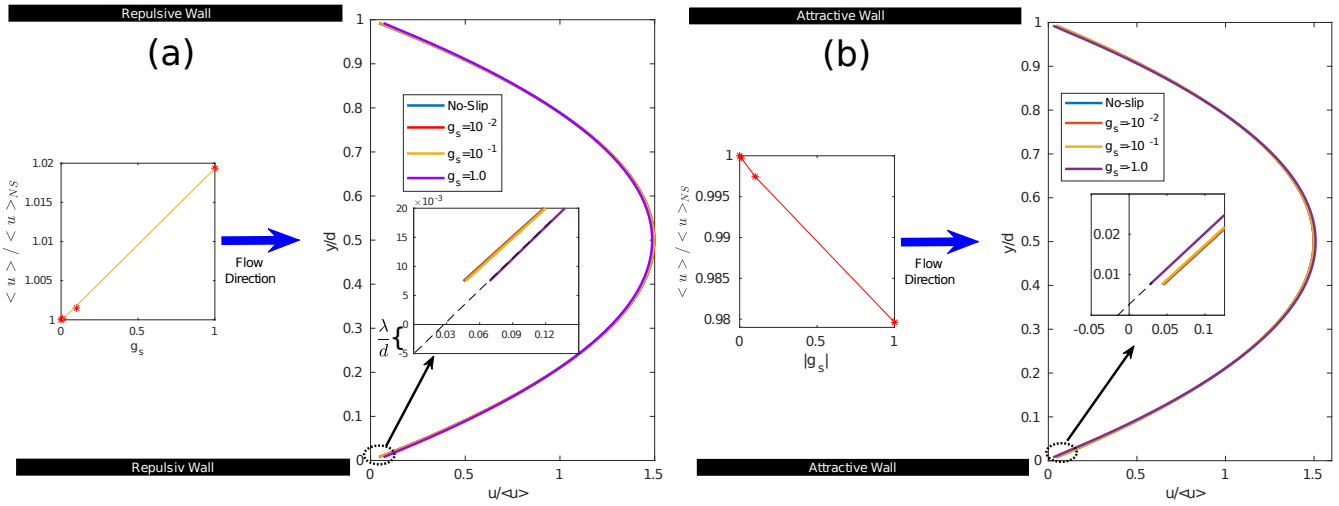

FIG. 3. Slippage of flow between repulsive (a) and attractive (b) walls, leading to positive and negative slip, respectively. The flow velocity profiles are shown in right-hand-side panels. The definition of slip length λ is shown in (a). The insets in left-hand-side panels show the mean velocity of flow versus the force factor g_s. The repulsive and attractive interactions resulted in enhanced (a) and decreased flow rates (b), respectively.

$2bL$. The eigenvalues α_n are obtained from

$$\cos \alpha_n = \lambda \alpha_n \sin \alpha_n. \tag{16}$$

The convergence is shown to be fast with a few terms needed for the required accuracy. The factor a_n is equal to

$$a_n = \frac{2 \sin \alpha_n}{\alpha_n + \sin \alpha_n \cos \alpha_n}. \tag{17}$$

The slip flow through ducts with polygonal cross-sections is solved using a collocation method by [82]. Those solutions presented in tables are illustrated in Fig. 5. The graph indicates that the flow is enhanced due to the slippage with higher rates as the number of sides in the cross-section of the duct becomes less. A triangular shape receives the highest rate of flow enhancement among the polygonal cross-sections while the circular shape possesses the lowest rate of flow increase.

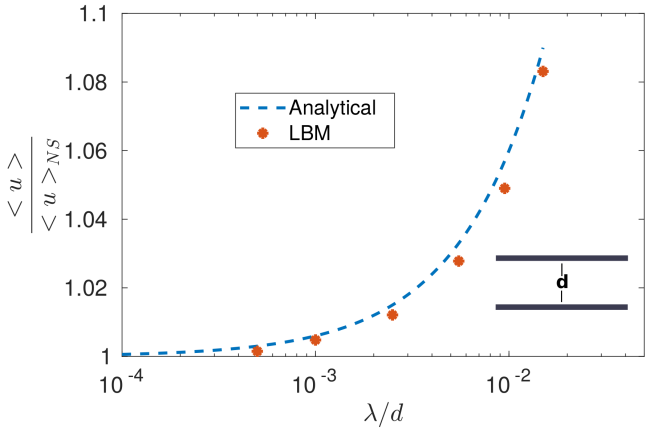

FIG. 4. Validation of slip flow simulations for Poiseuille flow between parallel walls. Normalized mean flow velocity as a function of normalized slip length. d is the plate separation. Our LBM results are shown along with the analytical line as driven by Eq. 14 (a linear equation shown in semi-log plot).

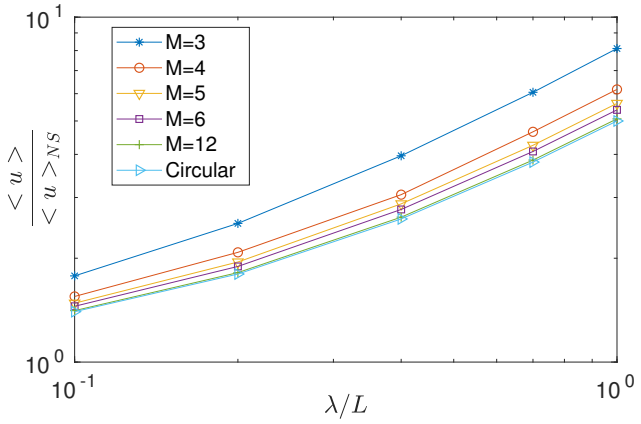

FIG. 5. Normalized mean flow velocity as a function of normalized slip length for polygonal ducts with M sides. Tabulated data obtained from Ref. [82] are transformed into the figure.

V. SUPERPOSITION METHOD FOR REHABILITATION OF SPURIOUS VELOCITIES

We propose a simple post-processing method to rehabilitate the velocity fields obtained from the LBM simulations of single-phase fluid interacting with active solid interfaces, *i.e.*, the surfaces with repulsive/attractive forces. The method is based on the linearity of the Navier-Stokes equations for Stokes flow. The full Naver-Stokes equation governing the isothermal incompressible fluid flow is [85]:

$$\rho\frac{D\vec{\boldsymbol{u}}}{Dt} = \rho\left(\frac{\partial\vec{\boldsymbol{u}}}{\partial t} + \vec{\boldsymbol{u}}.\nabla\vec{\boldsymbol{u}}\right) = -\nabla p + f + \mu\nabla^2\vec{\boldsymbol{u}} \quad (18)$$

$$\nabla.\vec{\boldsymbol{u}} = 0. \quad (19)$$

Here f is the body force (*e.g.* gravitational forces, ρg). For low Re, the full equation is simplified to Stokes equation of creeping and steady flow:

$$\nabla p - f = \mu\nabla^2\vec{\boldsymbol{u}} \quad (20)$$

$$\nabla.\vec{\boldsymbol{u}} = 0. \quad (21)$$

Since Stokes flow equations are linear, they are responsive to suitable methods in solving the linear partial differential equations such as linear superposition of solutions. Consider two flow systems (velocity and pressure fields, u_1, p_1 and u_2, p_2) individually satisfying Eqs. 20 ans 21. Then their linear combination could be solved with the superposition of the solutions of its components.

Based on this method, we construct a set of solutions for the rehabilitation of spurious currents. To fulfill the requirements of the superposition method, the spurious velocities are to be linear fields. We examine the applicability of a linear subtraction of the spurious velocities for a wide range of interfacial force strengths ($|g_s| \leq 2.5$). Furthermore, the linearity is generally held in low Re number flows. So we investigate a range of flow rates to give Re varying from below 1 to higher values up to 10, corresponding to a transition zone from Darcy to post-Darcy flow in porous media. The study would reveal to what extent the results of a superposition method could be valid for higher Re numbers (and also larger interfacial forces) where non-linearity may progressively appear.

The velocity fields required in order to implement the superposition method are as follows:

a) *Spurious velocity field* (u_{SP}):

This velocity field is obtained by simulation of the model incorporated with the interfacial forces, but all outer boundaries defined as periodic boundaries. We call this velocity field as u_{SP} hereafter. For example, if one models the flow by the gravity or using the velocity (or density) boundary conditions, to obtain the spurious velocity field, no gravity or boundary condition should be assigned. Therefore, the only velocity filed generated is due to the force imbalance called spurious velocities.

b) *Flow (original) simulation velocity field* (u):

This field is obtained from simulation of the same model, but with required configurations to generate the flow (whether velocity/density boundary conditions or gravitational forces). While simulations should be continued to reach the steady state, it is also vital to acquire the data from the same time step as one of the u_{SP} (with other simulation parameters kept the same, *i.e.*, the same lattice units). It is because the spurious velocities may vary with simulation time. This velocity field is called u here.

c) *Rehabilitated velocity field* (u^*):

The rehabilitated velocity field is then defined as

$$u^* = u - u_{SP} \quad (22)$$

i.e., the rehabilitated velocity vector on each lattice is calculated by subtraction of the spurious velocity vector from the flow original simulation velocity vector.

VI. VALIDATION OF SUPERPOSITION REHABILITATION METHOD: SLIP FLOW THROUGH CIRCULAR DUCTS

In addition to validation of the LBM code for slip flow simulations (as shown in Fig. 5), we also directly validate the introduced rehabilitation method when applied on a case with significant spurious velocities. For this purpose, the slip flow through a circular duct is modeled. The accuracy of the rehabilitated results for porous media simulations is also further assessed in the following sections.

The no-slip solution for flow velocity at radial distance r from the center of a circular duct is [80]

$$u = \frac{1}{4\mu}\left(R^2 - r^2\right)G \tag{23}$$

where R is the duct radius. The mean velocity is

$$\langle u\rangle = \frac{R^2}{8\mu}G \tag{24}$$

There is also a closed form solution for the slip flow through circular ducts as [81]

$$\langle u\rangle = \frac{R^2}{8\mu}\left(1 + \frac{4\lambda}{R}\right)G \tag{25}$$

When simulated numerically, curved surfaces of circular ducts induce large spurious velocities (see Fig. 6(a)). The superposition rehabilitation method results in quadratic profiles which are fully purified from parasitic velocities (Fig. 6(b)). Velocity profiles indicate the enhanced flow rates and the corresponding slip velocities as caused by interfacial repulsive forces (Fig. 6(c)). The slip lengths (λ) are also measured using quadratic fitting equations assigned to the velocity profiles. The rehabilitated flow fields (u^*) are used to calculate the flow rate enhancement versus the slip lengths (Fig. 6(d)). Despite significant spurious currents in original simulations, the rehabilitated results are proved valid with the close agreement to the analytical solution.

VII. SIGNIFICANCE OF SPURIOUS VELOCITIES IN POROUS MEDIA SIMULATIONS

In porous media LBM studies, the slip flow could be simulated using the interfacial forces while the main flow is generated using the boundary conditions or gravitational body forces. While the interplay of the surface forces and the main flow produces the slip behavior, it is important to estimate to what extent the simulations could be affected by the spurious velocities. We performed a general study on a typical porous medium comprised of monodispersed spheres with diameters equal to 68 cells. The surface forces characterized by the force factor of g_s are defined using SC and EFS models with an influence length of one cell. The distributions and magnitudes of spurious velocities are varied when using different force models. While the EFS model would reduce their magnitude, the spurious currents could yet cause entirely non-physical simulation results depending on the force factor strength and main flow rates assigned (see Fig. 7).

To study the severity of spurious currents, we extended the simulations to a range of flow rates and interfacial force strengths. The results are reported in l.u as shown in Fig. 8. When simulating a flow in porous media with a general flow velocity, $\langle u\rangle$, the magnitude of the spurious velocities could be estimated for weak to strong interfacial interactions using Fig. 8(a). In this study, the Reynolds number is equal to $\frac{\langle u\rangle d_p}{\nu} = 409 \times \langle u\rangle$ where d_p is the particle diameter and ν is kinematic viscosity. For instance, when using a surface force strength of $g_s = 1$, for simulations of laminar flow with $Re = 1$, the spurious velocities are on average 6 times as large as the mean flow velocity. As spurious velocities are almost constant for a certain g_s, this ratio increases when we simulate lower flow rates, causing non-physical results for entire Darcy flow range.

A unique relationship is found when the relative strength of spurious velocities is shown versus the ratio of $\frac{g}{g_s}$ (Fig. 8(b)). For the case of this study, the spurious velocities start to exceed the physical mean flow velocity when $\frac{g}{g_s}$ becomes smaller than the threshold of 2×10^{-4}.

VIII. SLIP FLOW THROUGH POROUS MEDIA

To evaluate the accuracy of our proposed method in the rehabilitation of the results affected by spurious velocities, we implement two different approaches:

First, using two different models to define the forces, we obtain various distributions of the spurious velocities. Although largely different from each other, the results of both force models before rehabilitation are totally non-physical velocity fields. Then we show the rehabilitated velocity fields obtained from both models match accurately in terms of both profiles and average values. The velocity fields with the interfacial interactions are featured with enhanced or reduced permeability (the mean flow velocity). The rehabilitation method is shown to reflect this behavior in an accuracy appropriate for the scale of the feature.

Second, a theoretical approach is employed by which an analogy between some simple systems and porous media is proposed. The simple systems are parallel plates and square ducts. In those systems, with only flat surfaces, the spurious velocities are known to be minimal. With the analogy proposed, we suggest that the general behavior of the systems should be similar. By comparing the macroscopic behavior, *i.e.*, the permeability of all systems in presence of repulsive and attractive surface forces, we validate the results attributed to simulated

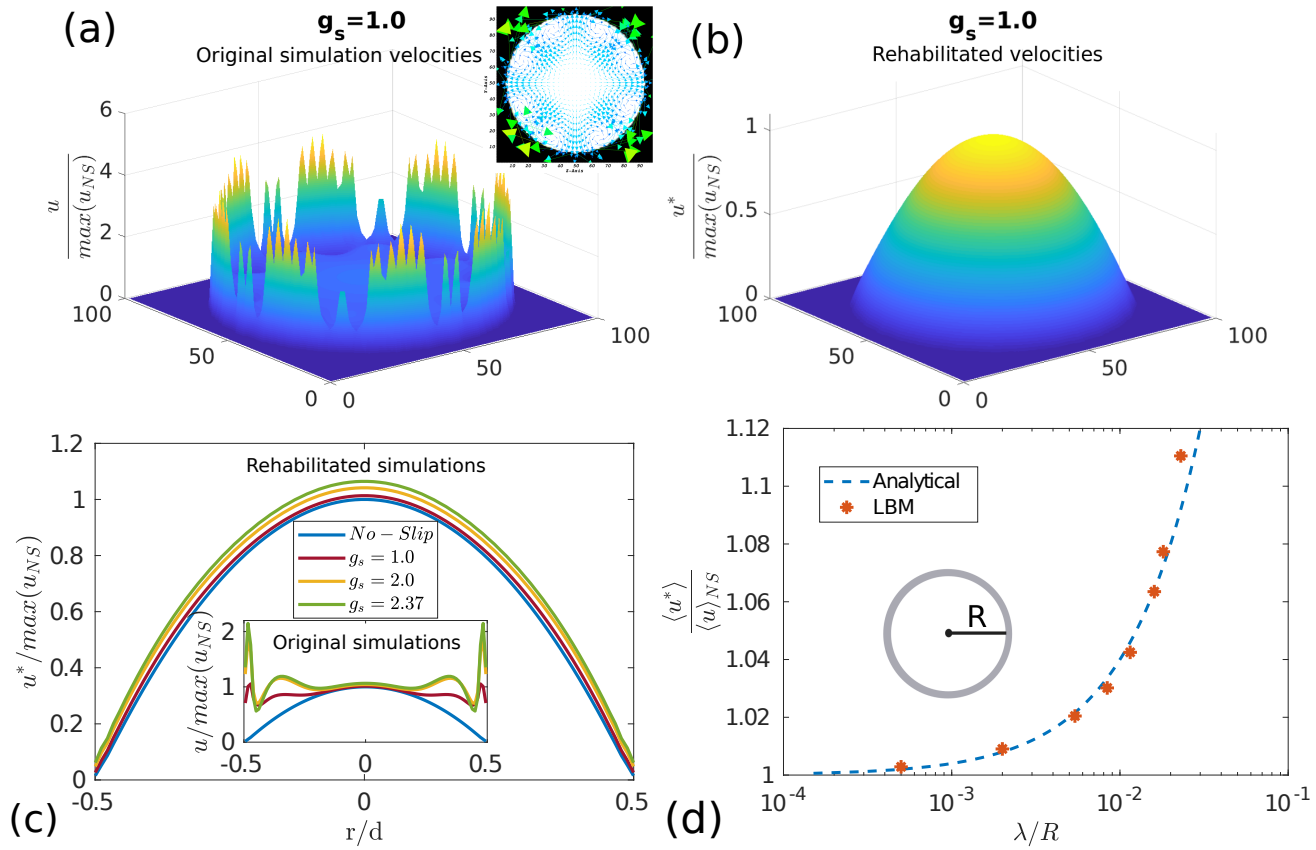

FIG. 6. Validation of superpositions rehabilitation method. Cross-sectional velocity profiles (a and b) for a circular duct with interfacial forces ($g_s = 1.0$). The diameter of the duct is equal to 90 cells where the resolution of the simulations is 99^3. The simulation velocities u are significantly affected by spurious velocities (a) with non-physical rotational velocities as shown in the inset at (a). The rehabilitation of flow leads to quadratic flow profiles (b). The simulation velocity profiles u are distorted by spurious velocities (inset at c) for $g_s > 0$. $d = 2R$ is the pipe diameter. The rehabilitated velocities u^* demonstrate the slippage of flow by increasing the force factor (c). The maximum velocity increases with flow slippage and the slip velocity at the duct surface leads to positive slip lengths. The LBM rehabilitated simulations for flow through circular duct are validated with the analytical solution as per Eq. 25 (d). The slip lengths (λ) are calculated using quadratic fittings on rehabilitated velocity profiles.

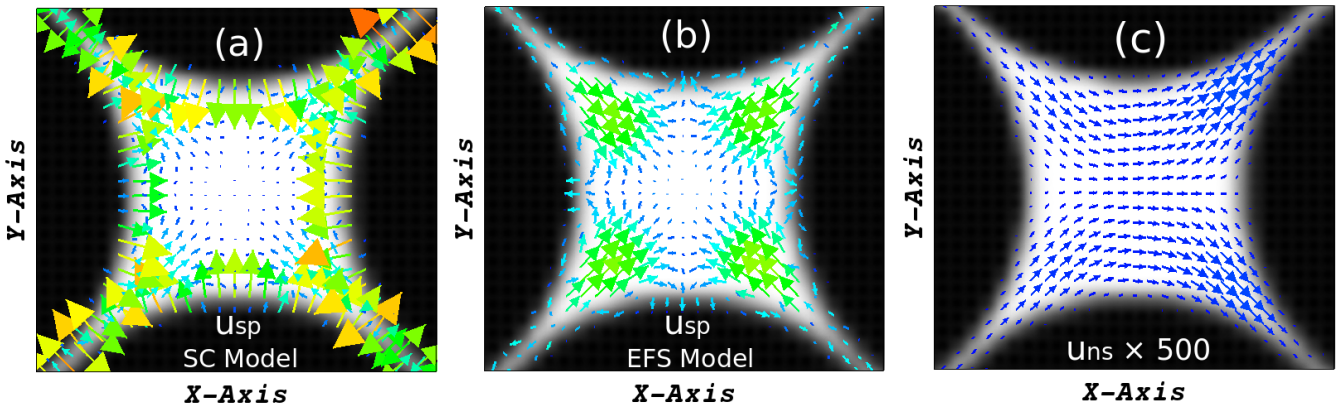

FIG. 7. Velocity vectors in a single pore space from a 3D porous medium showing spurious currents (a and b) and physical (no-slip) velocities (c). The net flow generated by gravity in x-direction has the mean flow velocity in a no-slip condition (without surface forces) equal to $\langle u \rangle_{NS} = 6.7 \times 10^{-5}$ ($Re = 0.027$). With an interfacial attractive force ($g_s = -2.0$) implemented in (a) and (b), the spurious velocities are dominant with different magnitudes and distributions for SC and EFS modes. The same medium with no-slip BC ($g_s = 0$) would result in a velocity field as shown in (c). Note the magnification scale in showing vectors in (c) for a comparison to spurious currents.

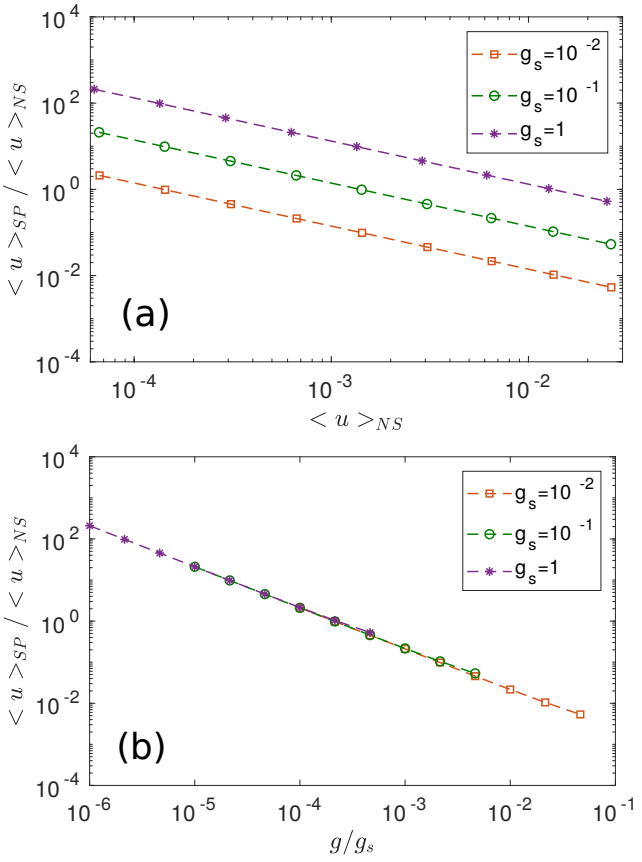

FIG. 8. Significance of spurious velocities in porous media simulations. The ratio of the mean of spurious velocities $\langle u\rangle_{SP}$ to mean velocity of no-slip flow $\langle u\rangle_{NS}$ for flow simulations through porous media where different intensities for solid-fluid interfacial forces (g_s) are assigned. The viscosity is equal to 0.1667. The pseudopotential SC model is used here. The characteristic length (sphere size) for the porous medium is 68 cells. A stronger interfacial force increases the spurious velocities (a). The velocity range in (a) is equivalent to $0.027 < Re < 10.7$. The relationship collapses into a unique behavior where the variation of velocities are shown versus the ratio of $\frac{g}{g_s}$ with g being the gravitational factor utilized to generate the main flow (b).

porous media flow rehabilitated using our superposition method.

A. Different interparticle-potential models

We performed simulations on a monodispersed porous medium comprised of spheres randomly distributed into a cube. Periodic boundary conditions are defined for the lateral sides of the model to account for infinite lateral sizes. The main flow is generated using a gravitational body force. Interfacial interactions are also implemented using SC and EFS models.

The idea is to show the independence of the rehabilitated velocity fields from the force model assigned (and hence the distribution of spurious velocities). To evaluate the suitability of the rehabilitation method for slip flow simulations, we also need to show that the resulted (rehabilitated) flow field is identical, both in average (macro-scale) and in velocity profile (pore-scale).

Porous media simulations for a wide range of flow velocities ($Re < 10.7$) corresponding to laminar and lower transition flow rates are performed (Fig. 9). Simulation mean flow velocities $\langle u\rangle$ are entirely non-physical for the whole flow range (even orders of magnitudes larger than the physical velocity), although yet largely dependent on the force model employed. The rehabilitated fields provide consistent flow behavior as expected (reduced flow with attractive force). The flow rates rehabilitated from both models are also identical, leading to a reduction factor of 0.915 in flow rate when $g_s = -1.0$. The force models alter the simulation velocities significantly, whereas the rehabilitated velocities out of them are closely similar with minor differences (Fig. 10).

In addition to macro-scale flow characteristics, *i.e.*, flow mean velocity, we also examine the accuracy of the proposed rehabilitation method for micro-scale velocity distributions. The porous media velocity profiles are shown for a small and large interfacial force strength ($g_s = -0.1$ and -2.0). Largely affected by spurious velocities, simulation velocities u (i-plots in Fig. 11) are much larger than physical (no-slip) velocities (iv-plots). However, the force models (SC and EFS) would influence the magnitudes and distributions of the spurious velocities (ii-plots). The rehabilitated velocity fields (iii-plots) are however not affected by the force model assigned, showing identical differences from the no-slip profiles (v-plots).

A pore velocity profile is also visualized along a straight line within the porous medium, where the simulation velocities obtained from two force models are shown to be dramatically different (i-plot in Fig. 12). The figure also demonstrates the rehabilitated velocities (ii-plot) and their difference from no-slip profiles due to the negative slip associated with attractive forces (iii-plot). The equivalence of profiles obtained from both models evidences the accuracy of the method in retrieving the slip flow velocities in characteristic scales.

B. Analogous systems

In this section, in a different approach, we evaluate the results obtained from rehabilitated simulations based on an analogy between porous media and other flow systems. Since the spurious velocities are known to be originated from non-planar surfaces, the analogous systems with planar surfaces are ideal. Thus we chose square ducts and parallel plates to resemble porous media. The macroscopic flow property, *i.e.*, the permeability is examined in all systems. Expressing the analogy based on the Kozeny-Carman conceptualization between those systems and porous media, we evaluate the permeabil-

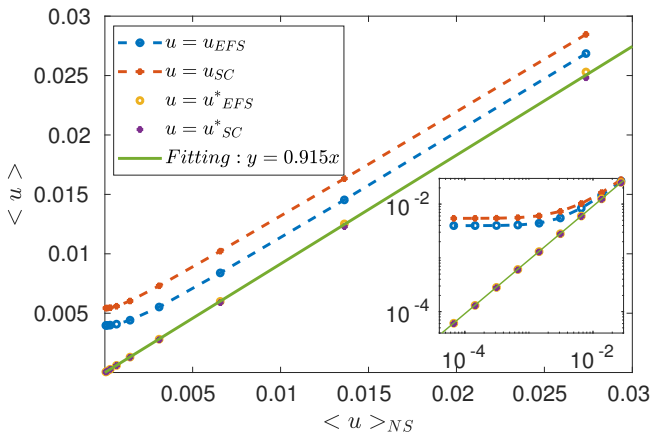

FIG. 9. Identical macroscopic results for different interfacial force schemes after using the rehabilitation method. The mean velocity, $\langle u \rangle$ of flow through porous media for $g_s = -1.0$ normalized by the mean velocity of the flow in the same model but with no-slip solid boundaries, $\langle u \rangle_{NS}$ ($g_s = 0$). $\langle u \rangle$ is the mean velocity of the original simulations and $\langle u^* \rangle$ denotes the mean velocity of the rehabilitated simulations using superposition method. Although EFS model provides an improvement in reducing the spurious velocities, the model results are mainly non-physical in the whole range of flow velocities. The inset is the same graph with logarithmic scales, showing that the model velocities could be several orders of magnitude larger than the physical velocities. The superposition rehabilitation method is shown to achieve the same feature (permeability reduction) regardless of the force model employed (SC or EFS) for the whole velocity range.

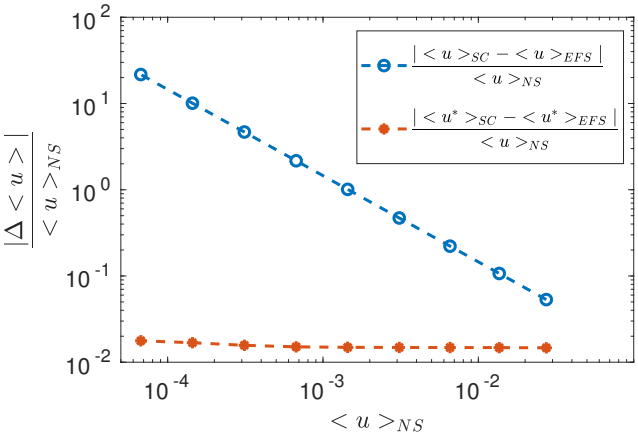

FIG. 10. The minor difference of rehabilitated velocities applied to different force schemes with the major difference in spurious velocities. The variation of the mean velocity of flow through porous media by using different force models (SC and EFS) for $g_s = -1.0$. $\langle u \rangle$ and $\langle u^* \rangle$ are the mean velocity of the original simulations and the simulations rehabilitated using superposition method, respectively. Using an improved force model (EFS) has changed the normalized magnitude of the spurious velocities up to more than one order of magnitude compared to the SC model. However, the rehabilitated velocity fields using superposition method (u^*) proved to be unaffected by the force model used, with a minor variation between different models.

ity variations due to interfacial forces in porous media. We argue that the results of porous media simulations when rehabilitated using our superposition method can be testified by comparing to analogous capillary ducts or parallel plates.

1. *Square ducts*

The Kozeny-Carman equation [86, 87] is the most widely used permeability model that relates the permeability to the medium's structural properties:

$$\kappa = \frac{\phi^3}{c(1-\phi)^2 S^2} \tag{26}$$

where c is the KC constant ($c = c'T^2$ with c' being an empirical constant and T, the flow tortuosity), ϕ is medium's porosity, and S is specific surface area, equal to the ratio of the total interstitial surface area to the bulk volume [85]. The KC model is based on transforming the porous medium into a bundle of capillary tubes with the same structural parameters, *i.e.*, the contact area of solids and fluids, and the volume of voids. Implementing the same approach, we transform our porous medium into square ducts. The interior surface area of ducts is to be equal to the solid surface area in porous media in contact with the fluid, A_{cont}:

$$A_{cont} = N(4a)lT \tag{27}$$

where N is the number of ducts and a is the duct cross-section side. The length of ducts is equal to lT where l is the length of the porous medium and T is the tortuosity of flow in porous media. The tortuosity of the flow was calculated using the following equation [88]

$$T = \frac{\sum u}{\sum u_L} \tag{28}$$

where u is the velocity magnitude and u_L is the velocity component in the longitudinal direction of flow ($T = 1.366$ for the modeled porous medium). The internal volume of the ducts is to be equal to the volume of voids in porous media, V_{void}:

$$V_{void} = Na^2lT \tag{29}$$

Substituting eq. 27 into eq. 29, we obtain the number of ducts and their side size as:

$$N = \frac{A_{cont}^2}{16V_{void}lT} \tag{30}$$

$$a = \frac{4Vvoid}{A_{cont}} \tag{31}$$

The mean flow velocity in a square pipe with no-slip boundaries is analytically shown to be equal to [80]

$$\langle u \rangle = \frac{a^2}{12\mu}\left[1 - \frac{192}{\pi^5}\sum_{i=1,3,5,\ldots}^{\infty}\frac{\tanh(i\pi/2)}{i^5}\right]G \tag{32}$$

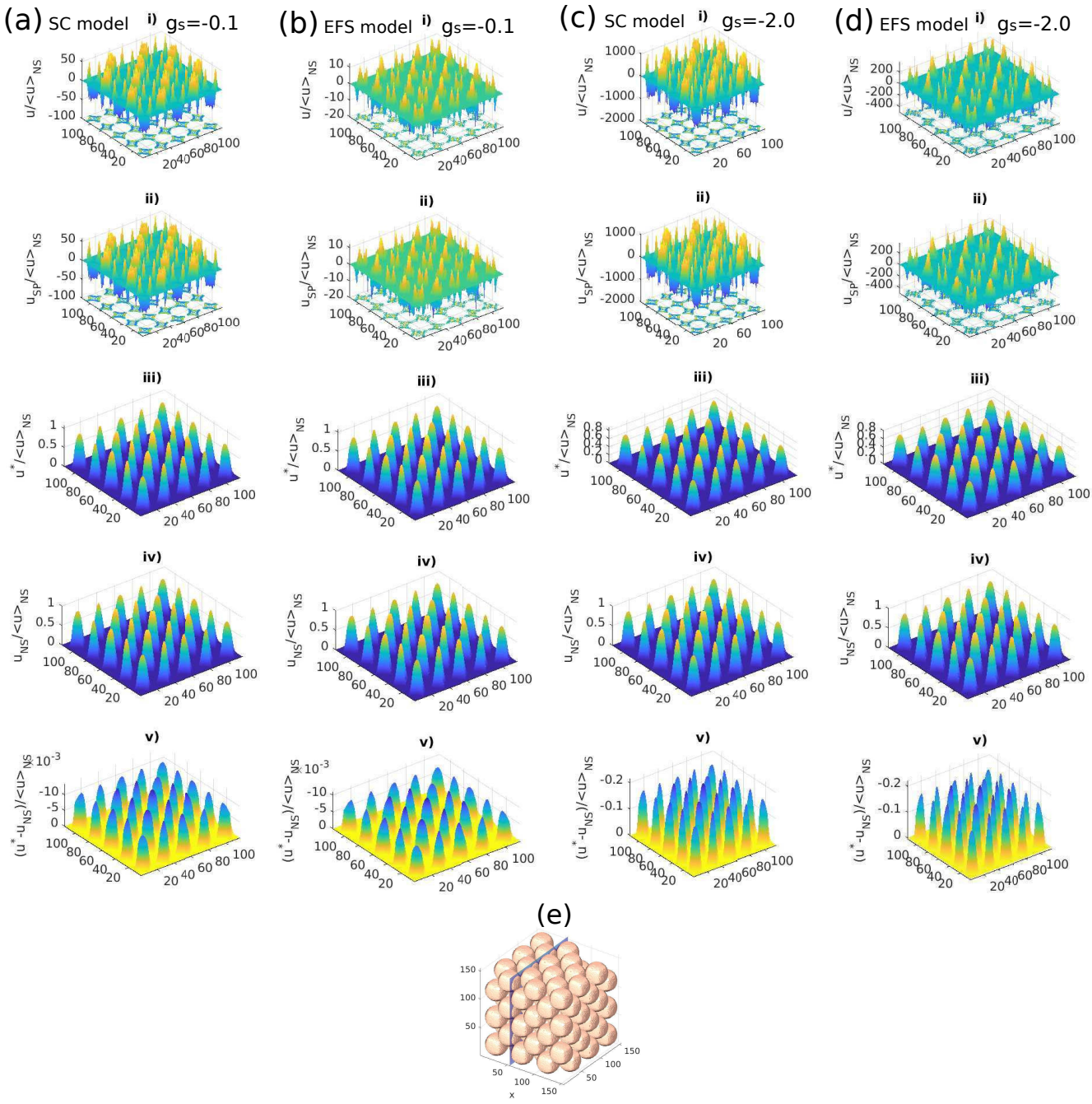

FIG. 11. Identical pore-scale results of different force schemes after rehabilitation. Velocity distributions shown across a cross-section perpendicular to the main flow direction through a 3D porous medium simulation. The surface force factor is $g_s = -0.1$ (a and b) and -2.0 (c and d) denoting interfacial attractive behaviours. The mean flow velocity in a no-slip condition (without forces) is $\langle u \rangle_{NS} = 6.7 \times 10^{-5}$ ($Re = 0.027$). The force models used are SC (a and c) and EFS (b and d). The simulation velocities, *i.e.*, u in i-plots are impaired with spurious velocities which are much larger than the physical velocities. u in SC model is also roughly 5-fold larger than that of EFS. The model of stagnant fluid (with only forces on interfaces) also resulted in similarly large velocities (spurious velocities, *i.e.*, u_{SP} in ii-plots), indicating the dominance of spurious velocities in the simulations. The results of our superposition rehabilitation method (u^* in iii-plots) are slightly different from those obtained from the model with no-slip boundaries ($g_s = 0$) illustrated as u_{NS} in iv-plots. The difference between u^* and u_{NS} is shown in v-plots where the pore flow velocities are reduced (less than %1 or %20 for $g_s = -0.1$ or -2.0, respectively) due to the attractive force effects. Despite the significant difference of simulation velocities (u) in two force models, the rehabilitation method resulted in accurately similar velocities both in quantities and distributions. We conclude that our rehabilitation model is capable to retrieve the small velocity changes due to surface force effects even for such complex interfaces with large spurious velocities. The 3D porous medium simulated is shown in (e) where the cross-section on which velocities are plotted is highlighted at x=55 and flow direction is in x.

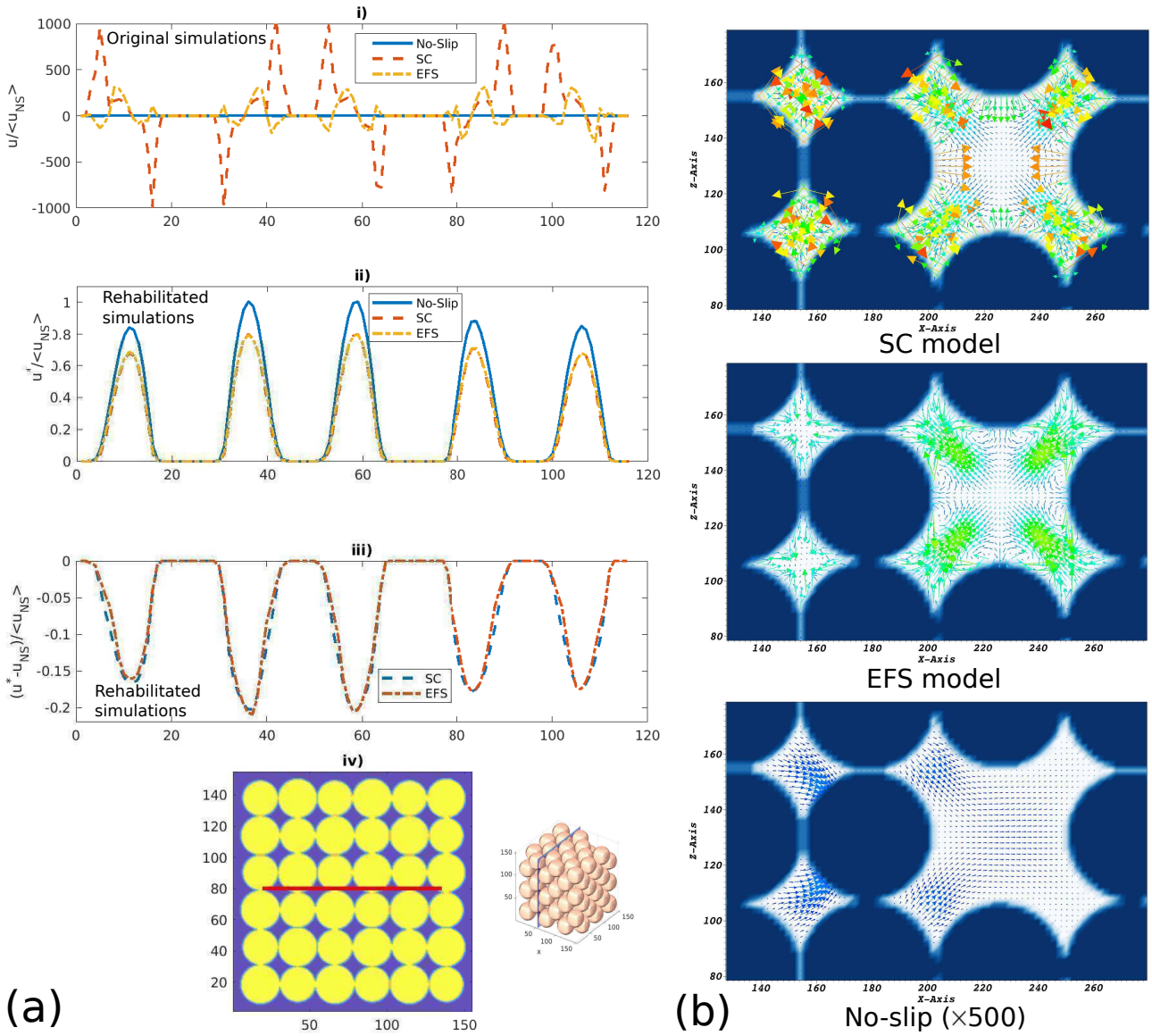

FIG. 12. Identical velocity profiles in pores after rehabilitation of spurious velocities from different force models. Velocity profiles (a) and vectors (b) for 3D porous media simulations where $\langle u \rangle_{NS} = 6.7 \times 10^{-5}$ ($Re = 0.027$). u in (a-i) is the simulation velocities for $g_s = -2.0$ simulated using SC and EFS models (D3Q15 scheme) as well as the model of no-slip BC ($g_s = 0$). u resulted from two models are entirely corrupted by spurious velocities. They are also largely different, both in values and distributions. Despite the differences in u, the rehabilitated velocities (u^*) of both models as shown in (a-ii) match accurately together indicating a flow pore-wide velocity reduction due to the effects of attractive forces on solid surfaces. The profile of the changes in velocities ($u^* - u_{NS}$) for both models is also shown in (a-iii) demonstrating the close agreement of the results of the models after rehabilitation. In (a-iv) are shown the line (in red) and the cross-section (in y-z plane perpendicular to the flow main direction, x) over which the velocity profiles are plotted. The cross-section is highlighted in the porous medium. Original simulation velocity vectors (u) for different models where spurious velocities dominate the flow field (before rehabilitation) in both SC and EFS models are shown in (b). The no-slip flow field is much smaller in magnitudes of velocities than the spurious fields (Note the magnification factor of 500)

.

Considering $\langle u \rangle = \frac{\kappa}{\mu} G$

$$\kappa = \frac{a^2}{12}\left[1 - \frac{192}{\pi^5} \sum_{i=1,3,5,\ldots}^{\infty} \frac{\tanh(i\pi/2)}{i^5}\right] = ca^2 \quad (33)$$

$$c \approx 0.0342 \quad (34)$$

We use the analytical solution of permeability for comparison to our simulations with no-slip assumptions.

2. Parallel plates

A similar analogy between porous media and parallel plates based on the KC model could be considered. Following the same approach as one described for square ducts, the structural parameters are determined so that the same contact area and volume of voids are retained for the porous medium and the system of parallel plates. Therefore:

$$A_{cont} = 2bTl \tag{35}$$
$$V_{void} = bdTl \tag{36}$$

where b is the plate width, and d is the plate separation. The length of plates is also chosen as Tl. Thus:

$$d = \frac{2V_{void}}{A_{cont}} \tag{37}$$
$$b = \frac{A_{cont}}{2Tl} \tag{38}$$

We recall the analytical solution for mean velocity of flow between parallel plates with no-slip surfaces as [80]

$$\langle u \rangle = \frac{d^2}{12\mu} G \tag{39}$$

Knowing that $\langle u \rangle = \frac{\kappa}{\mu} G$

$$\kappa = \frac{d^2}{12} = c' d^2 \tag{40}$$
$$c' = 0.0833 \tag{41}$$

The flow velocity versus body force, $\langle u \rangle - \rho g$ for the porous medium simulations rehabilitated using our superposition method is shown in Fig. 13(a). The analogous systems are also simulated when the same interfacial force strengths are assigned (Fig. 13(b) and 13(c)). The no-slip analytical solutions are also included. The slip flow LBM validation for parallel plates is also already provided as discussed in Fig. 4. The analogous systems exhibit a similar macro-scale behavior as one of the porous medium in permeability variation with interfacial forces.

As demonstrated in Fig. 14, the permeability of the analogous systems are constantly proportional to that of porous media for $g_s < 0$ (attractive forces). The ratio of the analogous systems' permeability to that of porous media is a factor of less than 3 for all conditions. This implies a reasonable analogy defined as the factor is comparable to the empirical constant included in the original KC formula to account for geometrical effects including tube (pore) shapes (see Table 1 in Ref. [89] for a list of recommended values).

The variation of permeability with attractive interfacial forces are almost similar for all systems (Fig. 15). However the permeability of analogous systems for repulsive forces (positive g_s) increases with higher rates as the system becomes less complex, *i.e.*, $(\frac{\kappa}{\kappa_{NS}})_{plates} > (\frac{\kappa}{\kappa_{NS}})_{ducts} > (\frac{\kappa}{\kappa_{NS}})_{porous\ media}$ (Fig. 14). This is in

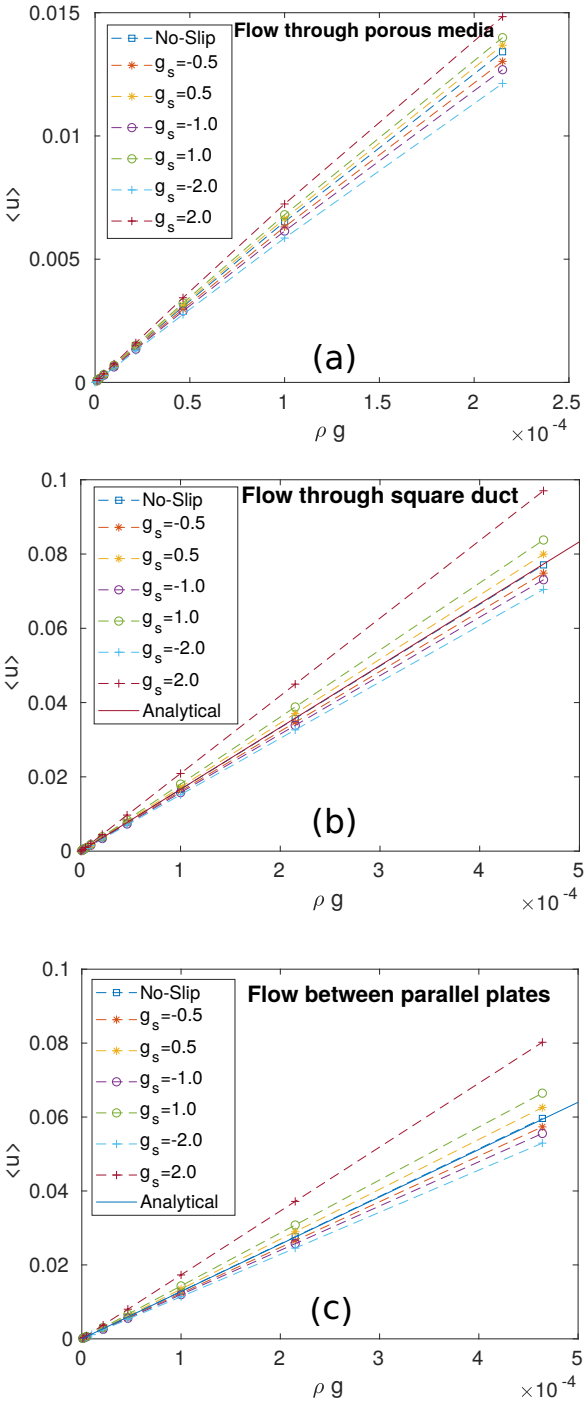

FIG. 13. Permeability variation due to interfacial forces. Flow mean velocity ($\langle u \rangle$) versus driving force (ρg) for the porous medium (a) and analogic systems composed of square ducts (b) and parallel plates (c). The results of porous media are rehabilitated using our proposed method. The general behaviour is enhanced and reduced permeability with repulsive (positive) and attractive (negative) surface forces, respectiveley as exhibited by all systems. The analytical solutions of the no-slip assumption for ducts and plates demonstrate the agreement of the results.

agreement with the analytical forms of slip flow as discussed in section IV and Fig. 5 .

In summary, we showed that the results of porous media simulations rehabilitated from spurious currents using our superposition method are in compliance with the results acquired from analogous systems. This approach demonstrated the reliability of the obtained results for porous media slip flow studies. The approach evaluated the rehabilitation method in obtaining macro-scale flow characteristics, in addition to the previous evaluation criterion (section VIII A) in which we examined the accuracy of the results both in pore-scale and as average.

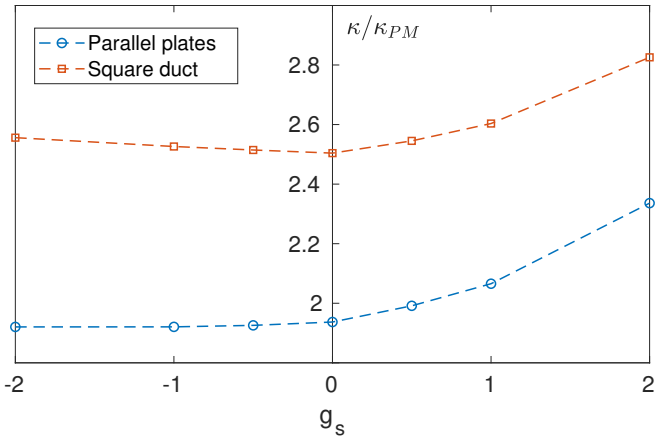

FIG. 14. The ratio of permeability of analogous systems (ducts and parallel plates) to that of the porous medium (κ_{PM}) versus surface force factor (g_s).

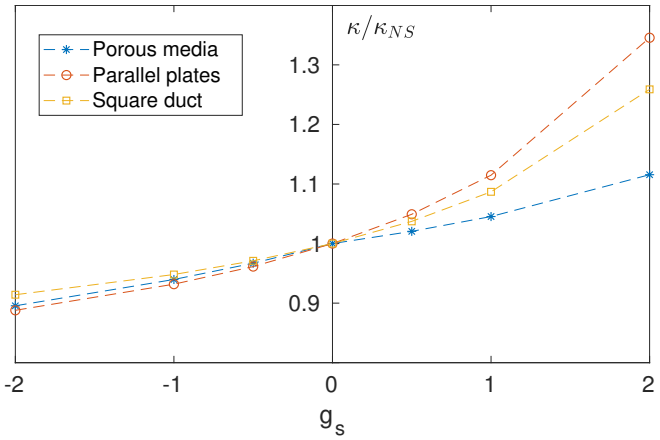

FIG. 15. Variation of the normalised permeability with the surface force factor (g_s). The permeability of the porous medium and its analogous systems reduces similarly with attractive interfacial forces. The permeability is enhanced with repulsive forces for all systems too, but with different rates.

IX. CONCLUSION

We investigated the slip flow behavior in porous media using the lattice-Boltzmann method. Firstly, the slip flow between parallel plates and ducts were examined. With repulsive and attractive interfacial forces, the flow rate enhances and reduces, respectively. From parallel plates to polygonal ducts, with the increase of the number of cross-section sides, the rate of flow enhancement due to repulsive forces diminishes. This is demonstrated by having a less flow enhancement for similar slip lengths in polygonal ducts with more sides. We showed the analytical solutions and our LBM simulations to explain the issue.

We also discussed the severity of the spurious velocities in case of porous media simulations due to the existence of force imbalance near the non-planar surfaces. To rehabilitate the simulations which are totally non-physical for entire Darcy range (up to $Re \approx 10$), we proposed a superposition method based on the linearity of simulations. The method was proved valid as shown to be closely in agreement with the analytical solution when applied on LBM simulation of slip flow through circular ducts.

To show the accuracy of simulated porous media flow results after rehabilitation, two strategies were employed:

First, using two different pseudo-potential force models, the spurious currents were shown to be altered significantly. Then we showed the equivalence of the rehabilitated results obtained from both models in the feature, *i.e.*, the scale of flow alteration due to interfacial forces. The approach verified the accuracy of the results in micro (pore)-scale (velocity profile) as well as macro-scale (permeability).

Second, using an analogy concept based on the Kozeny-Carman equation, we transformed our porous medium into simple structures, *i.e.*, parallel plates and square ducts in which spurious currents are negligible. Then we demonstrated the accuracy of the porous media rehabilitated results evidenced by the compliance with analogous systems. The compliance between the results of porous media and analogous systems was discussed in accordance with the analytical solutions. In this approach, we outlined the accuracy of superposition rehabilitation method in a macro-scale lookout.

The results revealed that the porous medium and the analogous systems are apparently similar in permeability reduction with attractive forces. However, the system of porous medium provides a smaller increase in permeability than analogous systems when the surfaces function as repulsive (causing positive slippage) with the same strength. This behavior inspires further research to investigate the differences in flow changes due to negative and positive slippage, with respect to the pipe (pore) shapes.

The study proposed a simple method to treat the LBM simulations affected by common spurious currents when interfacial interactions are investigated. The applications include the flow simulations when wettability is con-

cerned. Although examined for the LBM, the method is applicable to other fluid flow solvers dealing with linear Navier-Stokes equations. However, we note that the superposition method is tested here for the single-phase flow of incompressible fluid. The applicability of the method in the multi-phase flow where the phase separation is involved should be further evaluated.

[1] D. W. Green, G. P. Willhite, *et al.*, *Enhanced oil recovery*, Vol. 6 (Henry L. Doherty Memorial Fund of AIME, Society of Petroleum Engineers Richardson, TX, 1998).
[2] F. Javadpour, D. Fisher, M. Unsworth, *et al.*, Journal of Canadian Petroleum Technology **46** (2007).
[3] B. Metz, O. Davidson, H. De Coninck, M. Loos, and L. Meyer, *IPCC special report on carbon dioxide capture and storage* (2005).
[4] R. Juanes, E. Spiteri, F. Orr, and M. Blunt, Water Resources Research **42** (2006).
[5] M. A. Shannon, P. W. Bohn, M. Elimelech, J. G. Georgiadis, B. J. Mariñas, and A. M. Mayes, Nature **452**, 301 (2008).
[6] A. K. Kota, G. Kwon, W. Choi, J. M. Mabry, and A. Tuteja, Nature communications **3**, 1025 (2012).
[7] M. M. Pendergast and E. M. Hoek, Energy & Environmental Science **4**, 1946 (2011).
[8] U. Pasaogullari and C.-Y. Wang, Electrochimica Acta **49**, 4359 (2004).
[9] G. M. Whitesides, Nature **442**, 368 (2006).
[10] T. M. Squires and S. R. Quake, Reviews of modern physics **77**, 977 (2005).
[11] C. Cottin, H. Bodiguel, and A. Colin, Physical Review E **84**, 026311 (2011).
[12] E. Lauga, M. Brenner, and H. Stone, in *Springer handbook of experimental fluid mechanics* (Springer, 2007) pp. 1219–1240.
[13] C.-H. Choi, K. J. A. Westin, and K. S. Breuer, Physics of fluids **15**, 2897 (2003).
[14] D. C. Tretheway and C. D. Meinhart, Physics of fluids **14**, L9 (2002).
[15] C.-H. Choi and C.-J. Kim, Physical review letters **96**, 066001 (2006).
[16] E. Bonaccurso, M. Kappl, and H.-J. Butt, Physical Review Letters **88**, 076103 (2002).
[17] P. Joseph and P. Tabeling, Physical Review E **71**, 035303 (2005).
[18] T. A. Ho, D. V. Papavassiliou, L. L. Lee, and A. Striolo, Proceedings of the National Academy of Sciences **108**, 16170 (2011).
[19] K. P. Lee, H. Leese, and D. Mattia, Nanoscale **4**, 2621 (2012).
[20] K. Kikuchi and O. Mochizuki, Measurement Science and Technology **25**, 065702 (2014).
[21] A. Author, Lab on a Chip **7**, 299 (2007).
[22] W. Sparreboom, A. van den Berg, and J. C. Eijkel, Nature nanotechnology **4**, 713 (2009).
[23] W.-M. Zhang, G. Meng, and X. Wei, Microfluidics and nanofluidics **13**, 845 (2012).
[24] R. N. Moghaddam and M. Jamiolahmady, Fuel **173**, 298 (2016).
[25] M. Tschapek, Journal of Plant Nutrition and Soil Science **147**, 137 (1984).
[26] S. Doerr, R. Shakesby, and R. Walsh, Earth-Science Reviews **51**, 33 (2000).
[27] B. Chai, H. Yoo, and G. H. Pollack, The Journal of Physical Chemistry B **113**, 13953 (2009).
[28] J. Henniker, Reviews of modern physics **21**, 322 (1949).
[29] J.-m. Zheng and G. H. Pollack, Physical Review E **68**, 031408 (2003).
[30] J.-m. Zheng, W.-C. Chin, E. Khijniak, and G. H. Pollack, Advances in colloid and interface science **127**, 19 (2006).
[31] B. Chai and G. H. Pollack, The Journal of Physical Chemistry B **114**, 5371 (2010).
[32] M. Aminpour, S. Galindo-Torres, A. Scheuermann, and L. Li, Physical Review Applied **9**, 064025 (2018).
[33] E. Crevacore, T. Tosco, R. Sethi, G. Boccardo, and D. L. Marchisio, Physical Review E **94**, 053118 (2016).
[34] M. Aminpour, S. Galindo-Torres, A. Scheuermann, and L. Li, in *Scour and Erosion: Proceedings of the 9th International Conference on Scour and Erosion (Taipei, Taiwan, 5-8 November 2018)* (CRC Press, 2018) p. 161.
[35] N. Shahidzadeh-Bonn, A. Azouni, and P. Coussot, Journal of physics: condensed matter **19**, 112101 (2007).
[36] N. Shahidzadeh-Bonn, A. Tournié, S. Bichon, P. Vié, S. Rodts, P. Faure, F. Bertrand, and A. Azouni, Transport in porous media **56**, 209 (2004).
[37] W. G. Anderson *et al.*, Journal of Petroleum Technology **39**, 1 (1987).
[38] W. Owens, D. Archer, *et al.*, Journal of Petroleum Technology **23**, 873 (1971).
[39] N. R. Morrow *et al.*, Journal of Petroleum Technology **42**, 1 (1990).
[40] C. Cottin-Bizonne, J.-L. Barrat, L. Bocquet, and E. Charlaix, Nature materials **2**, 237 (2003).
[41] R. Seemann, M. Brinkmann, E. J. Kramer, F. F. Lange, and R. Lipowsky, Proceedings of the National Academy of Sciences of the United States of America **102**, 1848 (2005).
[42] A. Günther and K. F. Jensen, Lab on a Chip **6**, 1487 (2006).
[43] C. Neto, D. R. Evans, E. Bonaccurso, H.-J. Butt, and V. S. Craig, Reports on Progress in Physics **68**, 2859 (2005).
[44] L. Chen, Q. Kang, Y. Mu, Y.-L. He, and W.-Q. Tao, International Journal of Heat and Mass Transfer **76**, 210 (2014).
[45] J. Harting, C. Kunert, and H. J. Herrmann, EPL (Europhysics Letters) **75**, 328 (2006).
[46] R. Benzi, L. Biferale, M. Sbragaglia, S. Succi, and F. Toschi, EPL (Europhysics Letters) **74**, 651 (2006).
[47] L. Zhu, D. Tretheway, L. Petzold, and C. Meinhart, Journal of Computational Physics **202**, 181 (2005).
[48] J. Harting, C. Kunert, and J. Hyväluoma, Microfluidics and Nanofluidics **8**, 1 (2010).
[49] X. Shan, Physical Review E **73**, 047701 (2006).
[50] A. J. Wagner, International Journal of Modern Physics B **17**, 193 (2003).
[51] C. Pooley and K. Furtado, Physical Review E **77**, 046702

(2008).
[52] K. Connington and T. Lee, Journal of mechanical science and technology **26**, 3857 (2012).
[53] S. Ganesan, G. Matthies, and L. Tobiska, Computer Methods in Applied Mechanics and Engineering **196**, 1193 (2007).
[54] A. Kupershtokh, D. Medvedev, and D. Karpov, Computers & Mathematics with Applications **58**, 965 (2009).
[55] T. Inamuro, T. Ogata, S. Tajima, and N. Konishi, Journal of Computational physics **198**, 628 (2004).
[56] A. Cristea and V. Sofonea, International Journal of Modern Physics C **14**, 1251 (2003).
[57] A. Q. Raeini, M. J. Blunt, and B. Bijeljic, Journal of Computational Physics **231**, 5653 (2012).
[58] P. Yuan and L. Schaefer, Physics of Fluids **18**, 042101 (2006).
[59] Z. Yu, L.-S. Fan, *et al.*, Physical Review E **82**, 046708 (2010).
[60] A. A. Mohamad, *Lattice Boltzmann method: fundamentals and engineering applications with computer codes* (Springer Science & Business Media, 2011).
[61] S. Galindo-Torres, Computer Methods in Applied Mechanics and Engineering **265**, 107 (2013).
[62] M. Sukop, (2006).
[63] X. He and L.-S. Luo, Journal of statistical Physics **88**, 927 (1997).
[64] C. K. Aidun and J. R. Clausen, Annual review of fluid mechanics **42**, 439 (2010).
[65] D. d'Humières, Philosophical Transactions of the Royal Society of London A: Mathematical, Physical and Engineering Sciences **360**, 437 (2002).
[66] X. Shan and H. Chen, Physical Review E **47**, 1815 (1993).
[67] X. Shan and H. Chen, Physical Review E **49**, 2941 (1994).
[68] A. K. Gunstensen, D. H. Rothman, S. Zaleski, and G. Zanetti, Physical Review A **43**, 4320 (1991).
[69] M. R. Swift, W. Osborn, and J. Yeomans, Physical review letters **75**, 830 (1995).
[70] M. R. Swift, E. Orlandini, W. Osborn, and J. Yeomans, Physical Review E **54**, 5041 (1996).
[71] X. Shan and G. Doolen, Journal of Statistical Physics **81**, 379 (1995).
[72] M. L. Porter, E. Coon, Q. Kang, J. Moulton, and J. Carey, Physical Review E **86**, 036701 (2012).
[73] N. S. Martys and H. Chen, Physical review E **53**, 743 (1996).
[74] X. He, S. Chen, and G. D. Doolen, Journal of Computational Physics **146**, 282 (1998).
[75] C. Pan, L.-S. Luo, and C. T. Miller, Computers & fluids **35**, 898 (2006).
[76] X. He, Q. Zou, L.-S. Luo, and M. Dembo, Journal of Statistical Physics **87**, 115 (1997).
[77] B.-Y. Cao, M. Chen, and Z.-Y. Guo, International Journal of Engineering Science **44**, 927 (2006).
[78] J. Hyväluoma and J. Harting, Physical review letters **100**, 246001 (2008).
[79] L. Bocquet and J.-L. Barrat, Soft matter **3**, 685 (2007).
[80] F. White, *Viscous Fluid Flow*, McGraw-Hill international edition (McGraw-Hill Higher Education, 2006).
[81] B. Halperin, *Progress in low temperature physics*, Vol. 15 (Elsevier, 2005).
[82] C. Y. Wang, The Canadian Journal of Chemical Engineering **81**, 1058 (2003).
[83] W. Ebert and E. M. Sparrow (ASME, 1965).
[84] C. Wang, Journal of Fluids Engineering **134**, 094501 (2012).
[85] J. Bear, *Dynamics of fluids in porous media* (Courier Corporation, 2013).
[86] J. Kozeny, Royal Academy of Science, Vienna, Proc. Class I **136**, 271 (1927).
[87] P. C. Carman, Transactions-Institution of Chemical Engineeres **15**, 150 (1937).
[88] A. Koponen, M. Kataja, and J. Timonen, Physical Review E **54**, 406 (1996).
[89] T. Ozgumus, M. Mobedi, and U. Ozkol, Engineering Applications of Computational Fluid Mechanics **8**, 308 (2014).